Direct neutrino mass measurements after PLANCK

Physics of the Dark Universe 4 (2014) 75–80

Contents lists available at ScienceDirect

Physics of the Dark Universe

journal homepage: www.elsevier.com/locate/dark

Direct neutrino mass measurements after PLANCK

J.A. Formaggio

Laboratory for Nuclear Science, Massachusetts Institute of Technology, Cambridge, MA, United States

ARTICLE INFO

Keywords:
Neutrino mass
Beta decay
Electron capture
Cosmology

ABSTRACT

The absolute mass scale of neutrinos remains an open question subject to experimental investigation from both particle physics and cosmology. Over the next decade, a number of experiments from both disciplines will attempt to probe the mass scale further to the very limits of the predictions from oscillation results. This paper provides a broad overview of the experimental program in neutrino mass scale measurements, with a particular focus on direct experimental probes due to come online over the next decade.

1. Introduction

Two remarkable paradigm shifts have taken place over the past 15 years in neutrino physics and cosmology. With regard to neutrino physics – or, perhaps more precisely, on the question of neutrino mass – the field has shifted from "discovery" to "precision". Indeed, measurements gathered from solar [1–6], atmospheric [7], and reactor [8,9] neutrinos have shown conclusively that neutrinos change flavor and, as a consequence, have a very small but nonzero mass. The measurements on these oscillation parameters are now being probed at the few percent level. This last point is further accentuated by the fact that our knowledge of the mixing angle θ_{13} – unknown just a few years ago – is now one of the most precisely measured mixing parameter in the neutrino sector, with the most recent value reported to be $\sin^2(2\theta_{13}) = 0.095 \pm 0.010$ [10].

Almost concurrently, observational cosmology has made a similar phase transition into precision measurements; providing an outstanding view of the cosmos. Precision measurements on the energy and matter content and evolution of the universe now allowed detailed tests of cosmological models that were simply unavailable even a decade ago. We are finally reaching the stage where direct comparisons between neutrino masses as determined by cosmology and as determined by nuclear physics experiments are possible (see Table 1). This paper briefly surveys the experimental landscape for direct neutrino mass measurements (see Fig. 1).

2. The impact of cosmology

The imprint of cosmological neutrinos upon the structure evolution of the universe has become a testable aspect of cosmology in recent years. Although neutrinos comprise only a small fraction of the matter density of the universe, their contribution can have significant effects on late-times large structure formation. Furthermore, neutrinos occupy a unique niche in cosmology, for although they are considered relativistic at the time of decoupling, they transition to non-relativistic velocities at late times. As such, neutrinos occupy a unique probe into our understanding of the details of cosmic evolution that is simply not shared by other particles.

In the standard model of both particle physics and cosmology, the number of neutrino species is fixed,[1] so the primary unknown which pertains to neutrinos is their contribution to the matter–energy density of the universe:

$$\Omega_\nu h^2 = \sum_i n_{\nu,i} m_{\nu,i}, \tag{1}$$

where $n_{\nu,i}$ is the neutrino number density and $m_{\nu,i}$ is its corresponding mass. The sum is performed over all neutrino species. In standard neutrino cosmology, the neutrino number density is fixed from the neutrino and photon temperature (T_ν and T_γ) and density (n_γ) and it is expected to be equal for all neutrino species:

$$n_\nu = \frac{3}{4}\left(\frac{T_\nu}{T_\gamma}\right)^3 n_\gamma,$$

$$\Omega_\nu h^2 = \frac{\sum_i m_{\nu,i}}{93\ \text{eV}}.$$

Constraints using PLANCK's temperature map and WMAP polarization is able to constrain the sum of the neutrino masses to

[1] The number of neutrinos, of course, can be relaxed in these cosmological fits and such studies on N_{eff} are the subject of inquiry in a number of analyses. The reader is referred to other articles in these proceedings for further information.

E-mail address: josephf@mit.edu.

http://dx.doi.org/10.1016/j.dark.2014.10.004

Table 1
Impact of neutrino mass sensitivity level as obtained from beta decay measurements on nuclear physics and cosmology.

Mass Sensitivity	Scale	Impact
$m_\nu \sim 2$ eV (current sensitivity)	eV	Neutrinos ruled out as primary dark matter
$m_\nu \sim 0.2$ eV	Degeneracy	Cosmology, $0\nu\beta\beta$ reach
$m_\nu \sim 0.05$ eV	Inverted	Resolve hierarchy if null result
$m_\nu \sim 0.01$ eV	Normal	Oscillation limit

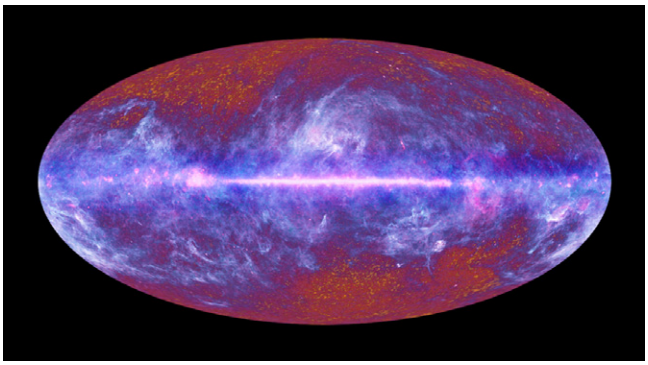

Fig. 1. The microwave all-sky as seen by the PLANCK satellite after one year of data taking.

below $\sum m_\nu < 0.933$ eV at 95% C.L [11]. Such limits become more stringent as when baryon acoustic data is included, spanning to $\sum m_\nu < 0.23$. Some tension between data sets exists (particularly with the Hubble parameter) that alters the extractable limits, and so the neutrino mass limits tend to vary to some degree depending on the data used and the exact model employed, but general results hover in the 0.2–1 eV range.

This landscape, however, is bound to improve over the next decade as large scale galactic surveys, polarization data, and weak lensing measurements continue to improve and expand. Indeed, next generation CMB satellites are likely to push well down into the inverted hierarchy region, perhaps even into the normal hierarchy scale [12]. However, with such a push, systematic uncertainties and small order corrections (for example, transitioning from the linear regime of the power spectrum to the non-linear regime) become increasingly important. The challenge then befalls both the observational community and the theoretical community in extracting neutrino mass limits (or observations) as new high precision data become available.

3. Direct neutrino mass measurements

Radioactive decay appears to be the most direct, model-independent approach for measuring the mass scale of neutrinos. Decay kinematics suffer neither from the inherent dependence on cosmological models, nor on the property of neutrinos necessarily being their own anti-particles. As such, this kinematic approach toward neutrino masses can be placed in direct comparison with the predictions from neutrino oscillations. Deviations from the prediction, for example via the existence of sterile neutrinos, can be readily tested.

Current and near-future experiments make use of one of the two decay mechanisms in order to probe the neutrino mass scale, particularly below 2 eV/c^2: β-decay and electron capture. In β-decay, the decay mechanism

$$(A, Z) \rightarrow (A, Z+1) + e^- + \bar{\nu}_e, \tag{2}$$

results in an energetic electron whose phase space depends on the neutrino mass:

$$\dot{N_\beta} = \frac{G_F^2 \cos^2\theta_c}{2\pi^3} |M_{\rm nucl}|^2 \cdot F(p_e, Z+1) \cdot E_e \cdot p_e \cdot E_\nu \cdot p_\nu. \tag{3}$$

Here, G_F is the Fermi coupling constant), θ_c is the Cabbibo angle, $|M_{\rm nucl}|$ is the nuclear matrix element, $E_e(p_e)$ is the electron total energy (momentum) and $E_\nu(p_\nu)$ is the neutrino energy (momentum). A small dependence on the electron charge distribution is captured via the Fermi function $F(p_e, Z)$, but the bulk of the spectral dependence is dictated by the phase space of the decay. As the cross-section depends explicitly on the neutrino momentum, the spectrum also carries information about the neutrino mass. It is often convenient to express the decay rate in terms of the electron's kinetic energy ($K_e \equiv E_e - m_e$), in which case the above formula becomes:

$$\frac{dN_\beta}{dK_e} = \frac{G_F^2 \cos^2\theta_c}{2\pi^3} |M_{\rm nucl}|^2 \cdot F(K_e, Z+1) \cdot (K_e + m_e) \cdot \sqrt{(K_e+m_e)^2 - m_e^2} \cdot (E_0 - K_e)^2 \cdot \Phi_\nu \tag{4}$$

$$\Phi_\nu = \sum_i |U_{ei}|^2 \sqrt{1 - \frac{m_{\nu,i}^2}{(E_0 - K_e)^2}} \cdot \Theta(E_0 - K_e - m_{\nu,i}) \tag{5}$$

where E_0 is the endpoint energy ($E_0 \equiv Q - E_{\rm recoil} - E_{\rm excitation}$) of the decay, Q is the parent–progeny mass difference from the decay, $E_{\rm recoil}$ is the recoil energy of the progeny, $E_{\rm excitation}$ is the excitation energy of the final state progeny, Θ is a step function imposed from energy conservation, and Φ_ν is meant to encapsulate the portion of the phase-space that depends explicitly on the neutrino mass scale, $m_{\nu,i}$. The spectrum is proportional to the incoherent sum of all neutrino couplings to the electron (weak) eigenstates, as determined by $|U_{ei}|^2$. As such, the process is sensitive to *all* $|U_{ei}|^2$ terms, including non-standard (i.e. sterile) states.

Although historically many different β-decay isotopes have been used, the focus has shifted in recent years to those with the lowest accessible endpoint, since the sensitivity to the neutrino mass scale improves with smaller values of E_0. These isotopes include ^{3}H (with an endpoint energy of 18.6 keV) and ^{187}Re (with an endpoint energy of 2.555 keV). Tritium, as a super-allowed transition, enjoys a relatively large mixing matrix with essentially no first-order dependence on the electron energy or angle. The endpoint energy requires a correction due to the excitation of the final state of the progeny nucleus, which for molecular targets such as T_2 can be non-negligible. Fortunately, calculations have been carried out and are expected to be known to be better than 1% [13]. Rhenium, despite its much lower endpoint value, is a first order forbidden transition, and thus has a much longer half-life and a more complex matrix element energy dependence.

The alternate process by which the neutrino mass scale can be probed is via electron capture

$$(A, Z) + e^- \rightarrow (A, Z-1) + \nu_e. \tag{6}$$

The differential decay rate is given by the expression

$$\frac{dN_{\rm EC}}{dK} = \frac{G_F^2 \cos^2\theta_c}{2\pi^3} \sum_x n_x C_x^n f_x (Q-K)^2 \times \frac{\Gamma_x}{2\pi} \frac{1}{(K-E_x)^2 + \Gamma_x^2/4} \cdot \Phi_\nu, \tag{7}$$

where n_x is the occupancy number of a given electron shell x ($n_x = 1$ for filled shells), C_x^n is a shape factor for a given transition with

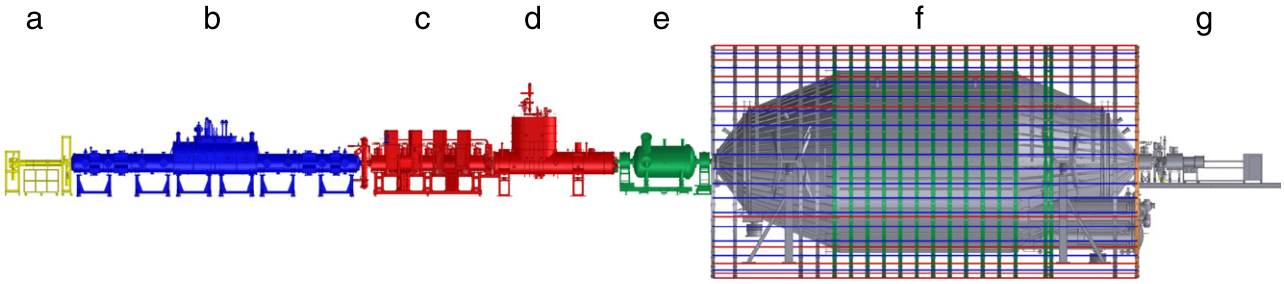

Fig. 2. Schematic overview of the 70-m KATRIN experimental beamline: (a) rear section, (b) tritium source, (c) differential-pumping section, (d) cryogenic-pumping section, (e) pre-spectrometer, (f) main spectrometer in air-coil framework, (g) focal-plane detector system.

angular momentum change, and f_x is defined as

$$f_x = \frac{\pi}{2}\beta_x^2 B_x \tag{8}$$

where β_x is the Coulomb amplitude of the bound-state electron radial wave-function and B_x is the correction due to the overlap between radial wave functions. The measured energy (K) represents the complete de-excitation energy of the progeny, distributed in terms of electrons and X-rays. Electron-capture has been a recent experimental focus of various calorimetric approaches, with ^{163}Ho often selected as the isotope of choice due to its allowed transition and low energy point energy.

4. Current techniques

4.1. MAC-E filters: The KATRIN experiment

Although the history of beta spectroscopy spans a variety of different magnetic and electrostatic spectrometers, this paper will concentrate mainly on the most recent experimental techniques. The technique which has demonstrated the greatest sensitivity to neutrino mass has been MAC-E-Filters (Magnetic Adiabatic Collimation with Electrostatic Filtering). This type of spectrometer, originally based on the work by Kruit [14] was later utilized by the Mainz [15] and Troitsk [16] experiments to probe the neutrino mass limits below 2 eV.

The MAC-E Filter combines the ability to retain a large fraction of electrons produced in beta decay with sufficient resolution to probe the endpoint of the decay spectrum. MAC-E Filters take advantage of the invariance of the magnetic moment of the electron:

$$\mu_e = \frac{p_\perp}{B} \simeq \text{constant}. \tag{9}$$

Under large, adiabatic changes of the magnetic field, μ_e remains constant. Thus, although electrons are originally ejected isotropically from the source, they can be relaxed such that their momentum is entirely oriented along the longitudinal direction. By imposing an electric field along the same direction, one can decelerate (and eventually reject) electrons with insufficient energy to overcome the electrostatic retarding potential (U). For an isotropic source, the resulting transmission function can be expressed analytically:

$$T(K_e, U) = \begin{cases} 0, & \text{for } K_e < qU \\ 1 - \sqrt{1 - \dfrac{K_e - qU}{K_e}\dfrac{B_s}{B_{\min}}}, & \text{for } qU < K_e < qU + \Delta E \\ 1 - \sqrt{1 - \dfrac{B_s}{B_{\max}}}, & \text{for } K_e > qU + \Delta E, \end{cases}$$

where B_S is the magnetic field strength at the source, $B_{\max}$ is the maximum (pinch) magnetic field strength, and ΔE is the resolution of the detector determined by the ratio of minimum to maximum magnetic field. The KATRIN experiment has optimized several aspects of the MAC-E Filter technique so as to reach an energy resolution of 0.93 eV.

KATRIN is designed to achieve an overall neutrino mass sensitivity of 200 meV at 90% C.L. after 3 years of data taking. Fig. 2 illustrates the overall components of the experiment, which include:

(a) A rear section, used for calibrating the response of the detector and monitoring the source strength during the run of the experiment,
(b) A Windowless Gaseous Tritium Source (WGTS), where 10^{11} electrons are produced per second by the decay of molecular high-purity tritium gas at a temperature of 30 K,
(c) An electron transport and tritium elimination section, comprising an active differential pumping (DPS) followed by a passive cryo-pumping section (CPS), where the tritium flow is reduced by more than 14 orders of magnitude,
(d) The electrostatic pre-spectrometer of MAC-E-Filter type, which offers the option to pre-filter the low-energy part of the tritium decay spectrum,
(e) The large electrostatic main spectrometer of MAC-E-Filter type which represents the precision energy filter for electrons, and
(f) A segmented Si-PIN diode array to count the transmitted electrons.

Further details on the experiment's design and performance parameters can be found elsewhere [17–19].

A number of elements of the KATRIN experiment have been commissioned in preparation for tritium running. Such elements include: (1) the large aircoil system, which fine tunes the magnetic field inside the main spectrometer and provides background suppression of electrons from the surrounding vessel walls; (2) successful bake-out and vacuum of the main vessel, down to 5×10^{-11} mbar; (3) installation and commissioning of the focal plane detector and, most recently, (4) first transmission of electrons through the main spectrometer, providing a successful demonstration of the MAC-E filtering technique down to the sub-eV precision level. Further commissioning of the main spectrometer will continue over the next year in preparation for tritium data taking in 2016 (see Fig. 3).

4.2. Calorimetric techniques: ECHO and HOLMES

Low temperature micro-calorimetry offers a complementary approach for measuring the neutrino mass scale. In a perfect calorimeter, the energy released from the decay – except for the neutrino energy – is fully absorbed. As such, the detector and the source are no longer distinct, and the detector becomes relatively insensitive to the details of the final state interaction or energy loss mechanism. Such a technique provides a distinct approach to that of MAC-E Filters, which are prone to the details of the energy loss mechanism and final state interactions.

Given the stringent requirements on the energy resolution necessary for β-spectroscopy, cryo-bolometers have been selected

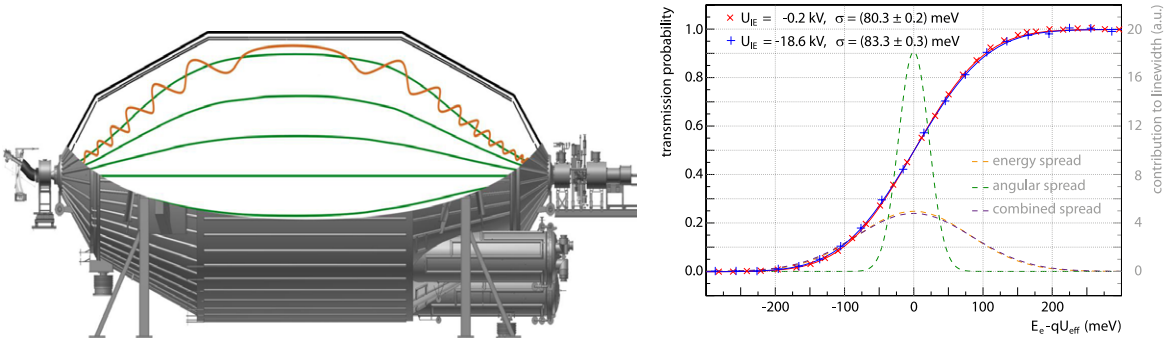

Fig. 3. Left: A schematic of the KATRIN detector during its first commissioning phase, with the electron source, the main spectrometer and detector connected in series. Right: The measured width of the KATRIN transmission function at two different retarding potentials (−0.2 and −18.6 kV). The above electron gun data is taken on axis with the main spectrometer. The width of the spectrometer transmission function is 0.93 eV if all angles from 0° to 51° contribute. The width of the transmission function for this on-axis measurement is dominated by systematics of the electron gun.

as the technology of choice for studying neutrino masses [20]. In calorimeters, the energy released from the decay (ΔE) translates into a change in temperature (ΔT) which is proportional to the heat capacitance $C(T)$ of the detector.

$$\Delta T = \frac{\Delta E}{C(T)_{\rm tot}} \exp^{-t/\tau}, \quad \text{with } \tau = \frac{C(T)}{G(T)}. \tag{10}$$

Here, $G(T)$ is the thermal conductance of the link between the absorber and the surrounding bath temperature. For superconductors below the critical temperature and for pure dielectric crystals, the heat capacitance is essentially dominated by phonon contributions and, as such, scales according to Debye theory:

$$C(T)_{\rm phonon} = \frac{12\pi^4}{5} N k_b \left(\frac{T}{\Theta_D}\right)^3 \tag{11}$$

where N is the number of atoms in the absorber, k_b is Boltzmann's constant, and Θ_D is the Debye temperature of the absorber.

The inherent energy resolution for this technique scales linearly with temperature and thus favors sub-kelvin operation:

$$\sigma_E \simeq \xi \sqrt{k_b T^2 C(T)} \tag{12}$$

where ξ is a dimensionless parameter. By accessing temperatures well below 1 K, bolometric detectors can reach eV scale energy resolution, opening the door for neutrino mass measurements. The original application of this technique was first used within the context of beta spectroscopy through the MARE experiment, using ^{187}Re imbedded in $AgReO_4$ as their main isotope for study. An initial neutrino mass limit of $\leq$15 eV/c^2 at 90% C.L. was obtained using very low mass detectors [21]. More recently, the focus has shifted from the beta decay of ^{187}Re to the electron capture decay of ^{163}Ho. Although possessing similar endpoint energies – 2.459 keV and 2.555 keV; respectively – the holmium decay is allowed rather than 1st forbidden and, as such, has a more favorable lifetime and simpler decay spectrum. Although the full atomic de-excitation process of the excited progeny state of ^{163}Dy is complex (X-ray emission, Auger electrons, Coster–Kronig transitions), the energy is eventually all transferred to the crystal, making the detector insensitive to such effects, at least to first order. The electron capture also provides an in-situ calibration of the energy scale, which aids the in-situ monitoring of the stability and response of these detectors.

The optimization of such bolometric detectors therefore focuses away from issues such as energy loss mechanism and final states to that of understanding the response of the detector itself. Most crucial to their performance will be the ability to resolve pile-up of electron capture events within the same detector. The rise times associated with such detectors is typically very slow (of order 1 μs), so large target activities cannot be tolerated without pile-up of events becoming a significant source of background near the endpoint of the electron-capture spectrum. Such difficulties are often overcome by either (a) improving the rise-time of the signal pulse or (b) distributing the target isotope across many detectors at once. In practice, both approaches are used in improving the sensitivity of the bolometric approach.

In recent years, two experimental programs have risen pursuing bolometric techniques: the ECHo [22] experiment (in Germany) and the HOLMES experiment (in Italy). Both use the electron capture process ^{163}Ho, but differ in the specific technology for detecting the rise in temperature. The ECHo experiment employs low temperature metallic magnetic calorimeters (MMCs) [23]. The temperature sensor of the MMCs consists of a para-magnetic alloy (Au:Er) which resides in a small magnetic field. A change in temperature leads to a change of magnetization of the sensor. A low-noise SQUID magnetometer detects the corresponding change in the magnetic flux and thus records the change in temperature/energy (see Fig. 4). MMCs have been shown to meet the timing and energy resolution requirements needed for a neutrino mass measurement. Furthermore, the technology can be multiplexed by coupling superconducting microwave resonators to a single SQUID, facilitating the deployment of multiple detectors. The ECHo experiment recently published an ^{163}Ho electron capture spectrum (see Fig. 4).

The HOLMES experiment, a follow up of the MARE project, was recently funded by the European Research Council with the goal of probing the neutrino mass scale using ^{163}Ho. HOLMES makes use of transition-edge sensors in order to measure the temperature rise due to energy deposition. TES detectors are a well established technology which routinely used optical, X-ray, microwave and dark matter searches [24]. TES detectors take advantage of the extremely sharp rise in resistivity as superconductors transition between superconducting and normal operation to detect small changes in temperature. Like MMCs, RF-SQUIDs will be deployed to simultaneously read out multiple detectors while keeping the number of readout channels fixed.

Both the ECHo and HOLMES collaborations aim for reaching the 0.2 to 2 eV/c^2 mass scale over the next several years. The final expected sensitivity of these experiments resides not merely on their technological approaches but also depends critically on the endpoint energy of the ^{163}Ho decay itself [25]. Lower endpoint energies impose less stringent requirements on the amount of holmium isotope required to achieve a certain level of statistical sensitivity. Currently, the uncertainties associated with the endpoint are large enough where the sensitivity ranges across an order of magnitude. Explicit investigation of the Ho–Dy mass difference over the next few years should help to more narrowly define the endpoint and determine the ultimate sensitivity of these two experiments.

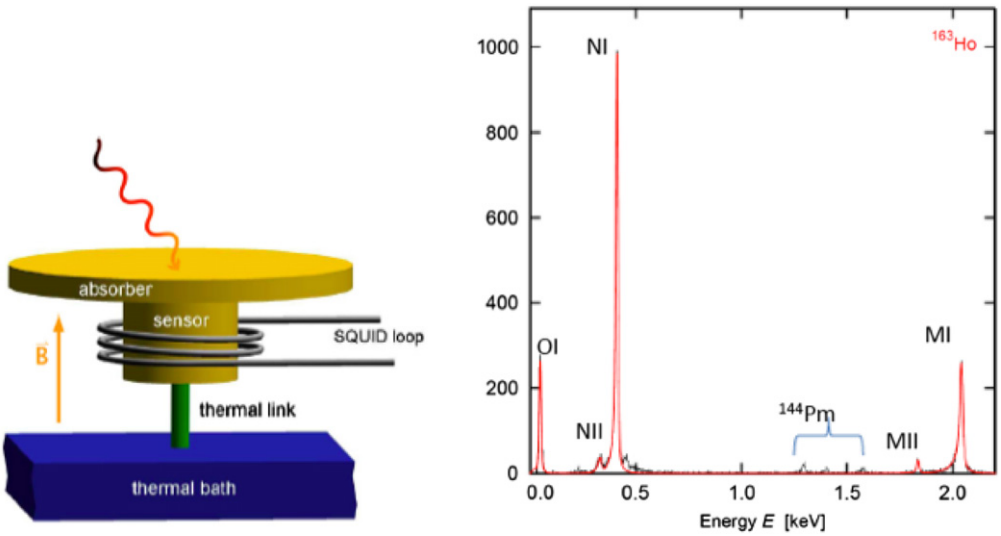

Fig. 4. Left: A schematic of the functionality of low temperature metallic magnetic calorimeters (MMCs). An electromagnetic interaction (X-ray, electron, etc.) deposits a small amount of energy, corresponding to a rise in temperature in the absorber. The change in temperature alters the magnetization of the sensor, which is detected by a low-noise SQUID magnetometer. Right: The electron capture spectrum from ^{163}Ho as measured by the ECHo experiment, with several de-excitation lines of dysprosium prominently visible.

4.3. Frequency techniques: Project 8

A final technique that has recently emerged for neutrino mass measurements makes use of relativistic cyclotron frequency as a means to extract the energy of the electron emitted from β-decay [26]. In a constant magnetic field, B, the corresponding cyclotron motion of the electron occurs at a frequency that depends on the kinetic energy (K_e) of the charged particle:

$$f_\gamma \equiv \frac{\omega_c}{2\pi\gamma} = \frac{1}{2\pi}\frac{eB}{m_e + K_e/c^2} \tag{13}$$

where $e(m_e)$ is the electron charge (mass) and f_γ is the radiated cyclotron frequency. The baseline angular frequency ω_c is $1.758820150(44) \times 10^{11}$ rad/s/T, which means at magnetic fields near 1 T, the emission is in the Ka microwave band. As the cyclotron frequency depends on the electron Lorentz factor, γ, it is dependent on the kinetic energy of the electron. The corresponding radiation emitted by the electron motion is small enough not to significantly affect the electron's energy, yet still carries the information of the kinetic energy itself.

For a freely-radiating electron undergoing cyclotron motion, the total power (P) radiated is given by the Larmor formula:

$$P = \frac{2}{3}\frac{q^2\omega_c^2 p_\perp^2}{m_e^2 c^3} \tag{14}$$

where $p_\perp$ is the relativistic transverse momentum of the trapped electron. For a 1 T magnetic field, the amount of power radiated by 30 keV electrons is approximately 1 fW. Although the emitted radiation is narrowband, the radiation as measured by a fixed receiver is more complicated, as it must take into account both Doppler shifts and coupling between the electron in the receiver, and in general will depend on the particulars of the chosen antenna configuration.

In the limit of a perfectly uniform magnetic field, the achievable resolution on the total predicted by this technique depends on the total observation time of the electron:

$$\Delta\omega = \Gamma \equiv \frac{1}{\tau} \tag{15}$$

where τ is the mean observation time of the electron. The frequency distribution is expected to follow a Lorentzian distribution whose width is determined by either the electron's mean free path or the cyclotron damping term. The inherent resolution will be further broadened according to the sampled field inhomogeneity, and the latter is typically what dominates the overall energy resolution.

Frequency techniques have the potential of combining the advantages of a gaseous source, such as employed in KATRIN, without needing to separate the source from the detector. The technique, however, does not enjoy the same established precedent as the other techniques. Thus both its feasibility and scalability need to be studied. To this effect, the Project 8 collaboration has constructed a prototype designed to detect the cyclotron emission from low energy electrons [27]. They use the isomeric decay of gaseous ^{83m}Kr as the source of electrons, as this provides near mono-energetic isotropic electrons with kinetic energies of 17.8 and 30.4 keV distributed throughout the sensitive volume. A superconducting solenoidal magnet provides the near 1 T magnetic field used for the detection, with a small coil used to create a magnetic bottle used to trap a fraction of ejected electrons. A WR42 rectangular waveguide section that looks directly into the electron cell couples to a cryogenic amplification system. For such a geometry, the cyclotron power couples primarily into the lowest propagating mode (TE_{10}) (see Fig. 5).

The prototype is constructed and data taking using ^{83m}Kr is to commence in summer, 2014.

5. Conclusions and outlook

The neutrino mass scale stands as a direct and unequivocal prediction of the observation of neutrino oscillations; a prediction that can be tested in both terrestrial and cosmological experiments. The precision obtained – and the projected precision expected over the next decade – by both of these approaches finally enables a qualitative comparison between them. In fact, it is not unreasonable to expect that in the not-too-distant future, cosmology and nuclear physics will be able to make quantitative predictions about the neutrino mass scale that can be effectively tested against one another. Such direct comparisons will do nothing but improve our knowledge of both neutrino properties and thermal cosmology.

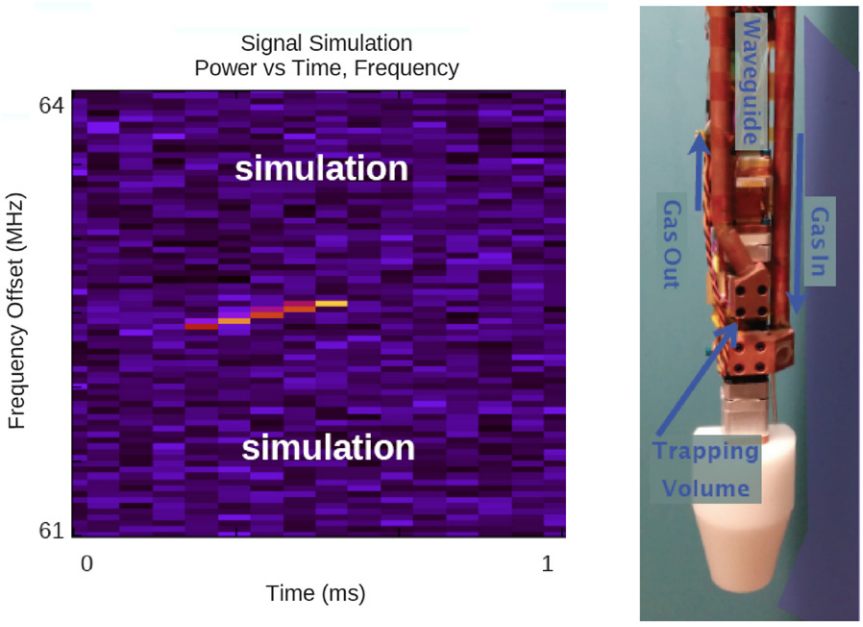

Fig. 5. Left: A simulation of the frequency signature of a trapped electron in the Project 8 prototype waveguide. A sudden burst of power in a narrow frequency range is expected, with a slight decay (rise) of the energy (frequency) over time. Right: A picture of the waveguide insert, where both the inlet krypton gas lines and trapping cell can be seen.

Acknowledgments

I would like to thank the members of the KATRIN, ECHo, HOLMES, and Project 8 collaboration for useful discussions with regard to the status of their respective experiments. J. Formaggio is supported in part by DOE Contract DE-FG02-06ER-41420.

References

[1] B. Cleveland, T. Daily, R. Davis Jr., J.R. Distel, K. Lande, et al., Measurement of the solar electron neutrino flux with the Homestake chlorine detector, Astrophys. J. 496 (1998) 505–526.
[2] J. Abdurashitov, et al., Measurement of the solar neutrino capture rate with gallium metal. III: Results for the 2002–2007 data-taking period, Phys. Rev. C 80 (2009) 015807.
[3] M. Altmann, et al., Complete results for five years of GNO solar neutrino observations, Phys. Lett. B 616 (2005) 174–190.
[4] K. Abe, et al., Solar neutrino results in Super-Kamiokande-III, Phys. Rev. D 83 (2011) 052010.
[5] B. Aharmim, et al., Low energy threshold analysis of the phase I and phase II data sets of the sudbury neutrino observatory, Phys. Rev. C 81 (2010) 055504.
[6] S. Davini, Precision measurement of the Be-7 solar neutrino rate and absence of day-night asymmetry in Borexino, Nuovo Cimento C034N06 (2011) 156–157.
[7] G. Mitsuka, et al., Study of non-standard neutrino interactions with atmospheric neutrino data in Super-Kamiokande I and II, Phys. Rev. D 84 (2011) 113008.
[8] S. Abe, et al., Precision measurement of neutrino oscillation parameters with KamLAND, Phys. Rev. Lett. 100 (2008) 221803.
[9] F. An, et al., Observation of electron–antineutrino disappearance at Daya Bay, Phys. Rev. Lett. 108 (2012) 171803.
[10] J. Beringer, et al., 2013 review of particle physics, Phys. Rev. D 86 (2012) 010001.
[11] P. Ade, et al., Planck 2013 Results, vol. XVI. Cosmological parameters, 2013.
[12] Y.Y. Wong, Neutrino mass in cosmology: Status and prospects, Ann. Rev. Nucl. Part. Sci. 61 (1) (2011) 69–98. URL: http://dx.doi.org/10.1146/annurev-nucl-102010-130252.
[13] A. Saenz, S. Jonsell, P. Froelich, Improved molecular final-state distribution of het+for the beta-decay process of t2, Phys. Rev. Lett. 84 (2000) 242–245. URL: http://dx.doi.org/10.1103/PhysRevLett.84.242.
[14] P. Kruit, F.H. Read, Magnetic field paralleliser for 2 electron-spectrometer and electron-image magnifier, J. Phys. E: Sci. Instrum. 16 (4) (1983) 313. URL: http://stacks.iop.org/0022-3735/16/i=4/a=016.
[15] C. Kraus, B. Bornschein, L. Bornschein, J. Bonn, B. Flatt, et al., Final results from phase II of the Mainz neutrino mass search in tritium beta decay, Eur. Phys. J. C 40 (2005) 447–468.
[16] V.N. Aseev, A.I. Belesev, A.I. Berlev, E.V. Geraskin, A.A. Golubev, N.A. Likhovid, V.M. Lobashev, A.A. Nozik, V.S. Pantuev, V.I. Parfenov, A.K. Skasyrskaya, F.V. Tkachov, S.V. Zadorozhny, Upper limit on the electron antineutrino mass from the troitsk experiment, Phys. Rev. D 84 (2011) 112003. URL: http://link.aps.org/doi/10.1103/PhysRevD.84.112003.
[17] G. Drexlin, V. Hannen, S. Mertens, C. Weinheimer, Current direct neutrino mass experiments, Adv. High Energy Phys. (2013) 293986.
[18] J. Angrik, et al., KATRIN Design Report 2004FZKA-7090, 2005.
[19] J. Amsbaugh, J. Barrett, A. Beglarian, T. Bergmann, H. Bichsel, et al. Focal-plane detector system for the KATRIN experiment, 2014.
[20] A. Giuliani, Neutrino physics with low-temperature detectors, J. Low Temp. Phys. 167 (5–6) (2012) 991–1003. URL: http://dx.doi.org/10.1007/s10909-012-0576-9.
[21] M. Sisti, C. Arnaboldi, C. Brofferio, G. Ceruti, O. Cremonesi, E. Fiorini, A. Giuliani, B. Margesin, L. Martensson, A. Nucciotti, M. Pavan, G. Pessina, S. Pirro, E. Previtali, L. Soma, M. Zen, New limits from the milano neutrino mass experiment with thermal microcalorimeters, Proceedings of the 10th International Workshop on Low Temperature Detectors, Nucl. Instrum. Methods Phys. Res. A 520 (13) (2004) 125–131. URL: http://www.sciencedirect.com/science/article/pii/S0168900203031814.
[22] L. Gastaldo, K. Blaum, A. Doerr, C.E. Düllmann, K. Eberhardt, S. Eliseev, C. Enss, A. Faessler, A. Fleischmann, S. Kempf, M. Krivoruchenko, S. Lahiri, M. Maiti, Y.N. Novikov, P. C.-O. Ranitzsch, F. Simkovic, Z. Szusc, M. Wegner, The electron capture ^{163}Ho experiment ECHo, J. Low Temp. Phys. (2014).
[23] P.-O. Ranitzsch, J.-P. Porst, S. Kempf, C. Pies, S. Schäfer, D. Hengstler, A. Fleischmann, C. Enss, L. Gastaldo, Development of metallic magnetic calorimeters for high precision measurements of calorimetric 187Re and 163Ho spectra, J. Low Temp. Phys. 167 (5–6) (2012) 1004–1014. URL: http://dx.doi.org/10.1007/s10909-012-0556-0.
[24] N.E. Booth, B. Cabrera, E. Fiorini, Low-temperature particle detectors, Ann. Rev. Nucl. Part. Sci. 46 (1) (1996) 471–532. URL: http://dx.doi.org/10.1146/annurev.nucl.46.1.471.
[25] A. Nucciotti, Statistical sensitivity of 163-Ho electron capture neutrino mass experiments, 2014, e-Print: arXiv:1405.5060.
[26] B. Monreal, J.A. Formaggio, Relativistic cyclotron radiation detection of tritium decay electrons as a new technique for measuring the neutrino mass, Phys. Rev. D 80 (2009) 051301.
[27] P. Doe, et al. Project 8: Determining neutrino mass from tritium beta decay using a frequency-based method, 2013.